Chinese Chemical Letters 35 (2024) 108708

Contents lists available at ScienceDirect

Chinese Chemical Letters

journal homepage: www.elsevier.com/locate/cclet

Exploring centimeter-sized crystals of bismuth-iodide perovskite toward highly sensitive X-ray detection

Xin Dong[a,b], Jing Liang[a,b], Zhijin Xu[b], Huajie Wu[b], Lei Wang[b], Shihai You[b,c], Junhua Luo[b,c,*], Lina Li[b,c,*]

[a] College of Chemistry, Fuzhou University, Fuzhou 350116, China
[b] State Key Laboratory of Structure Chemistry, Fujian Institute of Research on the Structure of Matter, Chinese Academy of Sciences, Fuzhou 350002, China
[c] University of Chinese Academy of Sciences, Beijing 100049, China

ARTICLE INFO

Article history:
Received 18 May 2023
Revised 15 June 2023
Accepted 19 June 2023
Available online 24 June 2023

Keywords:
Perovskite
Lead-free
Bismuth-based
X-ray detection
Sensitivity

ABSTRACT

Lead-halide perovskites exhibit outstanding performance in X-ray detection due to their intrinsic features such as high charge carrier mobility, large atomic number, and long carrier lifetime, but the toxicity of lead is regarded as the major factor hindering their development. Here, we introduce organic molecule (*R*)-(-)-2-methylpiperazine (*R*-MPz) into the bismuth-based structure to synthesize lead-free (*R*)-(H_2MPz)BiI_5 (*R*-MBI). The high-quality centimeter-sized single crystals have been obtained, which show a low dark current and superior environmental stability. Particularly, the single-crystal device of *R*-MBI exhibits a high $\mu\tau$ product up to 1.88×10^{-4} cm^2/V and a low trap density of 1.21×10^{10} cm^{-3}. Further, the detector displays excellent detection sensitivity of 263.58 μC Gy_{air}^{-1} cm^{-2} and a favorable low detection limit of 4.35 $\mu Gy_{air}/s$, both of which meet the requirement for medical diagnostics. These findings shed light on the exploration of innovative bismuth-based hybrid perovskites for high-performance X-ray detection.

X-rays are extensively utilized in security inspections, scientific research, and medical imaging due to their high penetration ability, short wavelength and high energy [1–6]. In principle, direct X-ray detection works by absorbing X-ray photons and converting them into electrical signals [7]. Based on the fundamental concept of X-ray energy conversion, the optimal detector provides the following key characteristics: a large atomic number (Z) with superior absorption of radiation; large carrier mobility, long charge lifetimes and low defect density to obtain effective carrier collection [8]. Currently, the conventional detection materials mainly include amorphous selenium (α-Se) [9], PbI_2 [10], CdTe [11], and Si [12], but these materials usually show inferior performance. For instance, the α-Se is restricted by its inadequate mobility-lifetime ($\mu\tau$) product (approximately 10^{-7} cm^2/V), resulting in poor sensitivity and detection limits [13]. In this situation, it is vitally desirable to explore new members of lead-free perovskites with low detection limits for high-sensitive X-ray detection.

In recent years, organic-inorganic hybrid perovskites have been proved to be ideal photodetection materials owing to their high carrier mobility, prolonged carrier lifetime, and low-cost single-crystal growth [14–18]. Among them, lead-based halide perovskites contain a high atomic number and thus exhibit outstanding X-ray absorption coefficients [19–23]. For example, it has been reported that sensitive detectors based on $MAPbI_3$ ($MA^+ = CH_3NH_3^+$) single crystal (SC) and $MAPbBr_3$ SC attain a sensitivity of 2.1×10^4 μC Gy_{air}^{-1} cm^{-2} [2,24], which is substantially greater than that of conventional α-Se X-ray detector [25]. However, with instability and hazardous Pb element, the potential of the above-mentioned compounds is significantly constrained [26]. In this situation, it is urgently desirable to explore lead-free hybrid perovskites as green X-ray detection materials. Bismuth, one of the nontoxic elements, has a large atomic number that will result in strong X-ray absorption [27], making it ideal for capturing charge carriers produced by X-rays [28]. The recently discovered one-dimensional (1D) (H_2MDAP)BiI_5 SC obtained a moderate sensitivity of 1 μC Gy_{air}^{-1} cm^{-2} at 5 V/mm [29], which provides the groundwork for improving the performance and demonstrates the potential for X-ray inspection. The direct X-ray detection was achieved in Bi-based perovskite (DMEDA)BiI_5 SC and exhibited a promising sensitivity of 72.5 μC Gy_{air}^{-1} cm^{-2} [30]. However, it needs to operate at a large field strength (494 V/mm), and its sensitivity and detection capability are insufficient [31]. Thus, it is

* Corresponding authors.
E-mail addresses: jhluo@fjirsm.ac.cn (J. Luo), lilina@fjirsm.ac.cn (L. Li).

https://doi.org/10.1016/j.cclet.2023.108708
1001-8417/

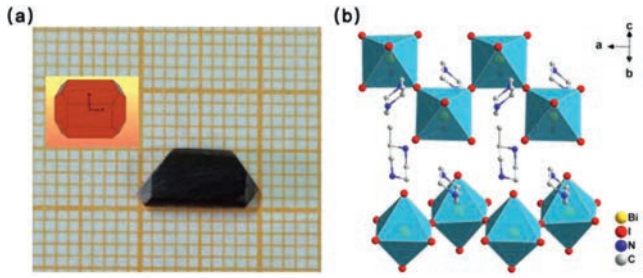

Fig. 1. (a) The simulated morphology based on the *R*-MBI SC (left) and solution-grown bulk crystal of *R*-MBI (right). (b) The crystal structure of *R*-MBI.

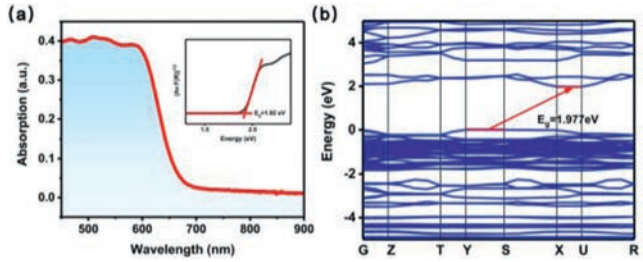

Fig. 2. (a) The optical absorption spectrum of *R*-MBI with the insert of corresponding Tauc plot. (b) The calculated energy band structure of the *R*-MBI.

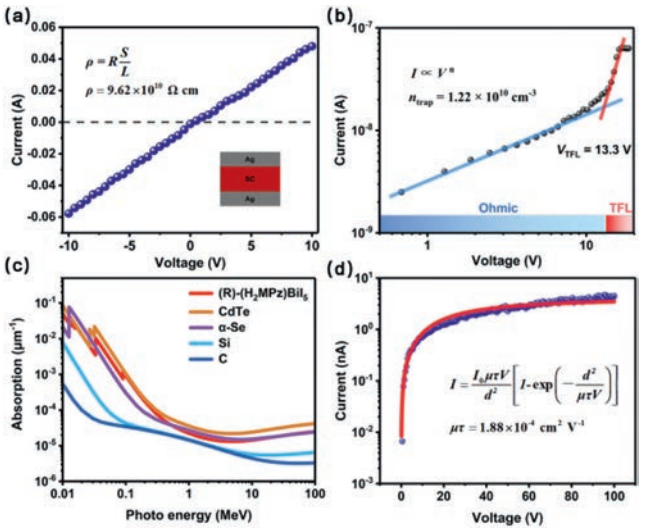

Fig. 3. (a) Bulk resistivity of *R*-MBI. (b) The *I-V* curve of *R*-MBI using the SCLC analysis. (c) Linear attenuation coefficient of *R*-MBI, CdTe, α-Se, Si, and C versus different X-ray photons energy. (d) Bias-dependent photoconductivity of *R*-MBI SC detector.

critical to develop X-ray detectors with great sensitivity to detect faint X-ray signals at low operating voltage.

In this research, we synthesized a non-lead compound (*R*)-(H_2MPz)BiI_5 (*R*-MPz = (*R*)-(-)-2-methylpiperazine, *R*-MBI) and demonstrated its suitability as an X-ray detector. The single crystal of *R*-MBI possessed a large bulk resistivity of 9.62×10^{10} Ω cm, and a high $\mu\tau$ product of 1.88×10^{-4} cm^2/V. Consequently, planar-structured crystal devices based on *R*-MBI SC are capable of excellent X-ray detection, producing an exceptional sensitivity of 263.58 μC Gy_{air}^{-1} cm^{-2} at 50 V/mm and detection limit less than 4.35 μGy_{air}/s. Our work demonstrates the *R*-MBI is a viable candidate for direct X-ray detection and inspires research into the next generation of eco-friendly detectors.

A centimeter-sized single crystal of $5 \times 10 \times 1.5\ mm^3$ (Fig. 1a) was grown *via* the low-temperature solution method. The powder X-ray diffraction (XRD) pattern of the *R*-MBI matches the simulated results quite well, implying the purity of crystals (Fig. S1 in Supporting information). Meanwhile, *R*-MBI exhibits no weight loss until 595 K and no significant change in the XRD pattern after 30 days, indicating favorable thermostability and long-term air stability (relative humidity, 70%) (Figs. S2 and S3 in Supporting information). Structural analysis indicates that *R*-MBI crystallizes in the orthorhombic ($P2_12_12_1$) space group (Table S1 in Supporting information), which forms a 1D zigzag chain along the *a*-axis with the BiI_6 octahedrons interconnected by corner-sharing units (Fig. 1b). In addition, the BiI_6 octahedra have a slight deformation, as shown by the non-uniformity of the Bi-I bond length and I-Bi-I angle. The Bi-I bond distance is in the range of 2.946 Å to 3.215 Å, while the I-Bi-I angle specifically falls between 83.80° and 176.58° (Fig. S4 and Table S2 in Supporting information). It is notable that organic component (*R*)-(-)−2-methylpiperazine cations are bonded to the 1D infinite zigzag chain *via* N–H···I hydrogen bonds (Fig. S5 in Supporting information).

The ultraviolet-visible diffuse reflectance spectra of *R*-MBI in the 450–900 nm region were carried out to evaluate the light-absorbing properties (Fig. 2a). The *R*-MBI exhibits an absorption cutoff wavelength of approximately 665 nm and the band gap is inferred with a value of 1.92 eV according to the Tauc curve (inset of Fig. 2a). Moreover, this band gap is relatively lower than that of several bismuth-based perovskites, including $(DFPIP)_4AgBiI_8$ (~2.03 eV) and $(NH_4)_3Bi_2I_9$ (~2.04 eV) [32,33]. As illustrated in Fig. 2b, the calculated band gap of *R*-MBI is 1.98 eV with the valence band maximum at point Y and the bottom of the conduction band at point U, indicating its indirect feature. Besides, the partial density of states spectra prove the *R*-MBI energy band gap is determined by the BiI_6 octahedra of the inorganic 1D chain (Fig. S6 in Supporting information): The conduction band minimum is predominantly assigned to the Bi-6p orbital, while the valence band maximum is principally attributable to the I-5p orbital.

The resistivity of *R*-MBI was calculated up to 9.62×10^{10} Ω cm (Fig. 3a), which is substantially higher than other lead-based perovskites (10^7–10^8 Ω cm) [2,19]. This high resistivity is advantageous in terms of lowering the dark current, resulting in a higher signal-to-noise ratio (SNR) [34]. Another significant parameter to evaluate the performance of semiconductors is trap density (n_{trap}). Thus, we measured the dark current-voltage (*I-V*) curve to investigate the n_{trap} of *R*-MBI by the space-charge-limited current method. The ohmic zone is denoted by the first smooth line in Fig. 3b, where the current signal grows linearly with voltage. As seen by the second steep line, the trap-filled area occurs when injected carriers fill the trap states. After that, we calculated the applied voltage at the intersection as the trap-filled limit voltage (V_{TFL}), which came out to be 13.3 V. The n_{trap} can also be determined from the following formula [35]:

$$n_{trap} = \frac{2\varepsilon\varepsilon_0 V_{TFL}}{eL^2} \quad (1)$$

where ε is the relative dielectric constant, ε_0 is the vacuum dielectric constant, e is the elemental charge, and L is the thickness. The relative dielectric constant ε ~11.8 of *R*-MBI was measured. After fitting calculation, the corresponding n_{trap} was determined to be 1.22×10^{10} cm^{-3}, which is considerably better than that of typical semiconductors Si ($n_{trap} = 10^{13}$–10^{14} cm^{-3}) and CdTe ($n_{trap} = 10^{11}$–10^{13} cm^{-3}) [36,37]. Such low trap density would increase charge transport ability, thus facilitating the acquisition of a high $\mu\tau$ product.

As previously stated, *R*-MBI possesses a low trap density, high resistivity, and the heavy element Bi, all of which are essential for an excellent X-ray detector. We used the NIST X-COM application to estimate the X-ray absorption coefficients of *R*-MBI and conventional semiconductors over a wide range of photon energies (0.01–

100 MeV) to examine the detection capacity of *R*-MBI [38]. In the entire energy range of interest, the absorption coefficient of *R*-MBI is comparable to that of α-Se and CdTe, and significantly superior to that of conventional silicon and carbon materials (Fig. 3c). Due to the high attenuation capacities ensuring adequate X-ray photon absorption, it is easier to collect charge carriers. As an X-ray detector, the $\mu\tau$ product is a crucial indicator to gain insight into the performance of the device, and a higher $\mu\tau$ product can collect more carriers at low electric fields [39]. The photocurrent-voltage curve of the *R*-MBI SC device is depicted in Fig. 3d, along with the accompanying fitting lines. The $\mu\tau$ product is calculated by the modified Hecht equation [40]:

$$I = \frac{I_0 \mu\tau V}{d^2}\left[1 - exp\left(-\frac{d^2}{\mu\tau}\right)\right] \quad (2)$$

where I_0 is the saturated photocurrent, d is the thickness, and V is the applied bias. Especially, *R*-MBI displays a relatively high $\mu\tau$ product of 1.88×10^{-4} cm^2/V, which is equivalent to the values for lead-based perovskites of (BDA)PbI_4 (4.43×10^{-4} cm^2/V) and $Cs_3Bi_2I_9$ (7.97×10^{-4} cm^2/V) [41,42].

As a result, we constructed an electrode with dimensions of $1 \times 2 \times 1.2\,mm^3$ to test the X-ray detection performance of *R*-MBI (Fig. 4a). By adjusting the X-ray tube current from 5 μA to 200 μA, the on/off photoelectric response was measured at different electric field strengths (Fig. 4b and Fig. S7 in Supporting information). The correlation between the response photocurrent and dose rates under various electric field strengths was depicted in Fig. 4c. The current density showed a nearly linear connection with the dosage rate of X-ray radiation, and the sensitivity could be calculated by measuring the slope of the linear relationship. Fig. 4d plots the computed X-ray detection sensitivity versus the electric field. The sensitivity of the *R*-MBI SC device is about 263.58 μC Gy_{air}^{-1} cm^{-2} at 50 V mm^{-1} resulting from the linear fit. This characteristic outperforms previously published bismuth-based 1D perovskite (DMEDA)BiI_5 detectors (72.5 μC Gy_{air}^{-1} cm^{-2} at 494 V/mm) and the double perovskite $(I\text{-}BA)_4AgBiI_8$ X-ray devices (5.38 μC Gy_{air}^{-1} cm^{-2} at 4.5 V/mm) [30,43]. Additionally, we examined the noise current by computing the standard deviation of the response current. In various field strength ranges, we calculated that the SNR was more than 3 when the dosage rate was 4.35 $\mu Gy_{air}/s$ (Fig. S8 in Supporting information) [34]. As a consequence, the lowest detectable dose rate of the *R*-MBI SC device is 4.35 $\mu Gy_{air}/s$, which is lower than the minimum dose rate needed for normal medical diagnosis (5.5 $\mu Gy_{air}/s$) [44,45]. Moreover, the photoelectric response to the X-ray was investigated by cycling the incident X-ray on and off at regular intervals (Fig. S9 in Supporting information), indicating that the output photocurrent was quite steady without obvious degradation.

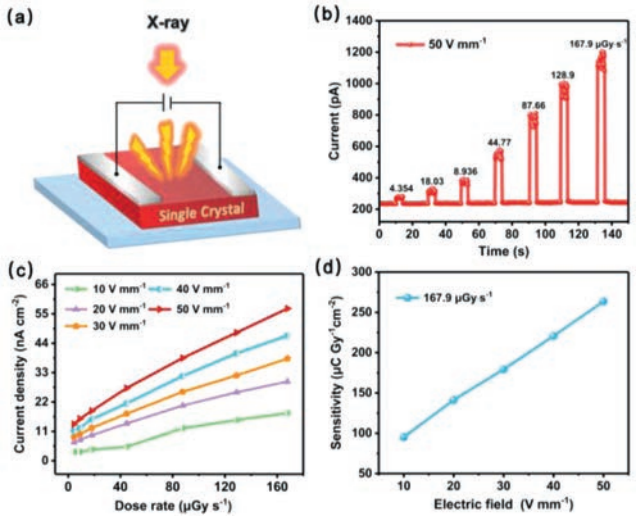

Fig. 4. (a) Device structure with *R*-MBI SC as the X-ray detector. (b) The photocurrent responses under different dose rates. (c) The relationship between photocurrent density and dose rate of *R*-MBI SC device at different field strengths. (d) Sensitivity under different electric fields of *R*-MBI SC detector.

In conclusion, we designed a lead-free bismuth iodide perovskite, (*R*)-$(H_2MPz)BiI_5$ (*R*-MBI), and centimeter-sized crystals were successfully acquired. Moreover, the features of low trap density, high attenuation efficiency and $\mu\tau$ product make the *R*-MBI single-crystal device exhibits high-sensitive X-ray detection with a superior sensitivity of 263.58 μC Gy_{air}^{-1} cm^{-2} at 50 V/mm. Besides, the *R*-MBI single-crystal detector displays a detection limit as low as 4.35 $\mu Gy_{air}/s$, meeting the dose rate required for medical diagnosis. This research advances the progress on high-performance bismuth-based perovskite X-ray devices and broadens the scope of environmentally friendly detectors for X-ray inspection.

Declaration of competing interest

The authors declare that they have no known competing financial interests or personal relationships that could have appeared to influence the work reported in this paper.

Acknowledgments

This work was financially supported by the National Natural Science Foundation of China (Nos. 22175177, 21971238, 22193042, 21833010, 22125110, 22122507, 21921001, and U21A2069), the Key Research Program of Frontier Sciences of the Chinese Academy of Sciences (No. ZDBS-LY-SLH024). The National Postdoctoral Program for Innovative Talents (No. BX2021315), and the National Key Research and Development Program of China (No. 2019YFA0210402).

Supplementary materials

Supplementary material associated with this article can be found, in the online version, at doi:10.1016/j.cclet.2023.108708.

References

[1] Y. He, C.C. Stoumpos, I. Hadar, et al., J. Am. Chem. Soc. 143 (2021) 2068–2077.
[2] H. Wei, Y. Fang, P. Mulligan, et al., Nat. Photonics 10 (2016) 333–339.
[3] J. Liu, B. Shabbir, C. Wang, et al., Adv. Mater. 31 (2019) 1901644.
[4] A. Sakdinawat, D. Attwood, Nat. Photonics 4 (2010) 840–848.
[5] Z. Liu, J.A. Peters, H. Li, et al., J. Electron. Mater. 44 (2015) 222–226.
[6] Y. Li, Y. Lei, H. Wang, et al., Nano-Micro Lett. 15 (2023) 128.
[7] Z. Xu, X. Liu, Y. Li, et al., Angew. Chem. Int. Ed. 58 (2019) 15757–15761.
[8] W. Yuan, G. Niu, Y. Xian, et al., Adv. Funct. Mater. 29 (2019) 1900234.
[9] S. Kasap, J.B. Frey, G. Belev, et al., Sensors 11 (2011) 5112–5157.
[10] Z. Gou, W. Liu, S. Huanglong, et al., IEEE Electron Device Lett. 40 (2019) 578–581.
[11] P. Duvauchelle, G. Peix, D. Babot, Nucl. Instrum. Methods Phys. Res. Sect. B 155 (1999) 221–228.
[12] M. Jeong, W.J. Jo, H.S. Kim, et al., Nucl. Instrum. Methods Phys. Res. Sect. A 784 (2015) 119–123.
[13] G. Belev, S.O. Kasap, J. Non-Cryst. Solids 345–346 (2004) 484–488.
[14] D. Yang, R. Yang, K. Wang, et al., Nat. Commun. 9 (2018) 3239.
[15] J.C. Blancon, J. Even, C.C. Stoumpos, et al., Nat. Nanotechnol. 15 (2020) 969–985.
[16] H. Wei, D. DeSantis, W. Wei, et al., Nat. Mater. 16 (2017) 826–833.
[17] X. He, Y. Deng, D. Ouyang, et al., Chem. Rev. 123 (2023) 1207–1261.
[18] L. Li, H. Chen, Z. Fang, et al., Adv. Mater. 32 (2020) 1907257.
[19] D. Shi, V. Adinolfi, R. Comin, et al., Science 347 (2015) 519–522.
[20] Y. He, L. Matei, H.J. Jung, et al., Nat. Commun. 9 (2018) 1609.
[21] S. Shrestha, R. Fischer, G.J. Matt, et al., Nat. Photonics 11 (2017) 436–440.
[22] C. Shan, F. Meng, J. Yu, et al., J. Mater. Chem. C 9 (2021) 7632–7642.
[23] W. Xu, M. Niu, X. Yang, et al., Chin. Chem. Lett. 32 (2021) 489–492.
[24] S. Yakunin, M. Sytnyk, D. Kriegner, et al., Nat. Photonics 9 (2015) 444–449.
[25] W. Wei, Y. Zhang, Q. Xu, et al., Nat. Photonics 11 (2017) 315–321.
[26] A. Babayigit, A. Ethirajan, M. Muller, et al., Nat. Mater. 15 (2016) 247–251.
[27] R. Mohan, Nat. Chem. 2 (2010) 336.

[28] R.E. Brandt, R.C. Kurchin, R.L.Z. Hoye, et al., J. Phys. Chem. Lett. 6 (2015) 4297–4302.
[29] K. Tao, Y. Li, C. Ji, et al., Chem. Mater. 31 (2019) 5927–5932.
[30] L. Yao, G. Niu, L. Yin, et al., J. Mater. Chem. C 8 (2020) 1239–1243.
[31] C. Ji, S. Wang, Y. Wang, et al., Adv. Funct. Mater. 30 (2020) 1905529.
[32] J.A. Steele, W. Pan, C. Martin, et al., Adv. Mater. 30 (2018) 1804450.
[33] C. Wang, H. Li, M. Li, et al., Adv. Funct. Mater. 31 (2021) 2009457.
[34] W. Pan, H. Wu, J. Luo, et al., Nat. Photonics 11 (2017) 726–732.
[35] Q. Cui, X. Song, Y. Liu, et al., Matter 4 (2021) 2490–2507.
[36] J.R. Ayres, J. Appl. Phys. 74 (1993) 1787–1792.
[37] A. Balcioglu, R.K. Ahrenkiel, F. Hasoon, J. Appl. Phys. 88 (2000) 7175–7178.
[38] M.J. Berger, J.H. Hubbell, S.M. Seltzer, et al., XCOM: photon Cross Sections Database: NIST Standard Reference Database 8 (NIST), https://www.nist.gov/pml/xcom-photon-cross-sections-database, accessed.
[39] Y. Liu, H. Ye, Y. Zhang, et al., Matter 1 (2019) 465–480.
[40] J. Androulakis, S.C. Peter, H. Li, et al., Adv. Mater. 23 (2011) 4163–4167.
[41] Y. Shen, Y. Liu, H. Ye, et al., Angew. Chem. Int. Ed. 59 (2020) 14896–14902.
[42] Y. Zhang, Y. Liu, Z. Xu, et al., Nat. Commun. 11 (2020) 2304.
[43] Z. Xu, H. Wu, D. Li, et al., J. Mater. Chem. C 9 (2021) 13157–13161.
[44] D.R. Douglas, M. Bopaiah, Health Phys. 79 (2000) S20–S21.
[45] I. Clairand, J.M. Bordy, E. Carinou, et al., Radiat. Meas. 46 (2011) 1252–1257.